https://doi.org/10.5194/egusphere-2026-578
Preprint. Discussion started: 6 February 2026

Evaluating SCIAMACHY-retrieved and ECHAM-simulated stratospheric aerosol characteristics by their comparison after volcanic eruptions

Christine Pohl[1,a,*], Ulrike Niemeier[2,*], Alexei Rozanov[1], Felix Wrana[3], and Christian von Savigny[3]

[1]Institute of Environmental Physics, University of Bremen, Bremen, Germany
[2]Max Planck Institute for Meteorology, Hamburg, Germany
[3]Institute of Physics, University of Greifswald, Greifswald, Germany
[a]now at Department of Physics, Lund University, Lund, Sweden
[*]These authors contributed equally to this work.

Correspondence: Christine Pohl (christine.pohl@fysik.lu.se) and Ulrike Niemeier (ulrike.niemeier@mpimet.mpg.de)

Abstract.

Satellite observations and global aerosol–micropysical model simulations are essential to study the impact of volcanic aerosols on stratospheric composition and dynamics. However, despite their continuous improvements, uncertainties remain in satellite retrievals and model outputs due to assumptions about aerosol size, composition, and simplified model parameterizations. The SCIAMACHY v2.0 PSD algorithm for obtaining stratospheric aerosol characteristics assumes a fixed particle number density profile representative of background conditions. MAECHAM5-HAM simulations employ parameterized aerosol microphysics and chemistry. Both approaches might be affected by increased uncertainties after volcanically perturbed situations. We compare SCIAMACHY v2.0 PSD aerosol extinction coefficient and effective radius profiles with MAECHAM5-HAM simulations following the Manam (2004/2005) and Sarychev (2009) eruptions to evaluate both data products. SCIAMACHY retrievals and MAECHAM5-HAM simulations show strong consistency for the Sarychev eruption in plume location, particle growth within the plume, and size reduction at plume boarder. In contrast, SCIAMACHY observes the Manam plume further north, with differences in aerosol size evolution compared to MAECHAM5-HAM simulations. Additional comparisons with SAGE II and alternative SCIAMACHY retrievals after the Manam eruption confirm that the v2.0 PSD approach provides the most realistic aerosol characteristics from SCIAMACHY. A model parameter study highlights the importance of accurate background aerosol size information, its parameterization, and vertical injection profiles for realistic simulations of volcanic plumes. Nudging MAECHAM5-HAM with ERA5 reanalyis data improves the simulated atmospheric dynamics and brings the simulation output closer to observations. Increasing the horizontal injection area compensates for under-represented chemical interactions involving OH and volcanic ash. These findings provide valuable insights for improving the simulations of volcanic eruptions with aerosol-microphysical models and enhancing the interpretation of satellite-based aerosol data.

https://doi.org/10.5194/egusphere-2026-578
Preprint. Discussion started: 6 February 2026

1 Introduction

Stratospheric sulfate aerosols from volcanic eruptions significantly influence the Earth's radiative and energy balances. These aerosols scatter solar short-wave radiation and absorb long-wave terrestrial radiation (Solomon et al., 2011; Kremser et al., 2016). Scattering leads to a cooling of the Earth's surface due to reduced solar radiation (Zanchettin et al., 2016) and absorption to heating of the stratosphere altering the atmospheric dynamics (Timmreck and Graf, 2006; Toohey et al., 2014; Niemeier et al., 2021). Aerosol-cloud interactions after long-lasting low-level eruptions can affect the physical and optical properties of clouds (Malavelle et al., 2017; Haghighatnasab et al., 2022). In addition, aerosols can cause stratospheric ozone destruction (Solomon, 1999; Robock, 2000; Zhu et al., 2018), reducing UV absorption and stratospheric heating. Depending on the strength of the eruption, the injection rate, the altitude, and duration, volcanic sulfur emissions can cool the Earth's surface for up to three years, temporarily compensating for anthropogenic climate warming (McCormick et al., 1995; Hegerl et al., 2003; Robock, 2000; Timmreck, 2012; Schmidt et al., 2018; Marshall et al., 2022).

Understanding the impacts of volcanic aerosols on the climate system requires both satellite observations and climate model simulations. Satellite instruments provide long-term global measurements of sulfur dioxide (SO_2) and stratospheric aerosol properties, such as concentrations, aerosol sizes, number concentrations, extinction coefficients, and optical depths. These data sets enable a direct estimation of aerosol radiative forcing. They also provide an important input for climate model simulations (Carn et al., 2017; Axebrink et al., 2024) and are essential to validate model results (e. g., Quaglia et al., 2023).

Earth system model (ESM) and general circulation model (GCM) simulations enhance our understanding of the role of volcanic sulfate aerosols in the climate system. While ESMs simulate the climate impact of volcanic aerosols, they often rely on prescribed aerosol optical properties (Zanchettin et al., 2016). Therefore, these models do not provide detailed information about aerosol formation in volcanic clouds. These processes can be simulated by coupling ESMs with an aerosol microphysical module (e. g., Niemeier et al., 2009; Aquila et al., 2012; English et al., 2013; Brenna et al., 2021). The module simulates the evolution of the aerosols, such as particle formation and growth, as well as their radiative interactions. This allows the study of stratospheric aerosol feedback mechanisms, between particle formation and the consequent dynamic impacts due to the heating of absorbed radiation (Aquila et al., 2014; Niemeier et al., 2021). Thus, models that include aerosol microphysics can be used to quantify stratospheric aerosol forcing and to investigate associated dynamical and microphysical interactions.

Substantial progress has been made in both satellite-based observations and model simulations quantifying the impact of volcanic aerosols in the stratosphere. On the observational side, satellite retrieval algorithms have recently been refined to reduce uncertainties in retrieval products (e. g., Rozanov et al., 2024). In addition, novel retrieval approaches have been developed to retrieve aerosol properties from existing satellite instruments (e. g., Rieger et al., 2014; Wrana et al., 2021; Bernath et al., 2023; Boone et al., 2024; Knepp et al., 2024; Pohl et al., 2024) and new satellite instruments in orbit (e. g., Eisinger et al., 2024). Currently, a limited number of satellite retrieval algorithms provide aerosol size information (e. g., Bernath et al., 2023; Wrana et al., 2023; Knepp et al., 2024; Pohl et al., 2024). Since the aerosol size is a key determinant of radiative forcing and climate impact - governing aerosol growth, sedimentation, evaporation and thus aerosol lifetime in the stratosphere, as well as radiative scattering, - these satellite retrieval products are of significant importance to the scientific community. On the modeling side,

https://doi.org/10.5194/egusphere-2026-578
Preprint. Discussion started: 6 February 2026

continuous improvements in input data sets and parameterization of microphysical, physical, and chemical processes aim to improve consistency with observed aerosol properties and radiative forcing (Tilmes et al., 2023).

Despite continuous improvement, discrepancies persist between model simulations. Variations in aerosol formation are the result of differences in the simulated particle sizes (Lacis et al., 1992; Laakso et al., 2022, 2024) and plume transport of the volcanic cloud (Quaglia et al., 2023). Accurate modeling of the transport processes is essential, since they represent critical components in the simulation performance. Differences in vertical air advection in the tropics can result in different aerosol lifetimes, different sulfate concentrations and particle sizes, and different impact on stratospheric dynamics (Niemeier et al., 2023). Additional sources of simulation discrepancies include the variability of circulation responses to volcanic eruptions (Timmreck, 2012; McGraw et al., 2016; Quaglia et al., 2023), injection profiles (Axebrink et al., 2024), and different treatments of aerosol microphysics (Laakso et al., 2022) and chemical processes (Clyne et al., 2021), for example, prescribed or simulated concentration of hydroxide radical (OH), which is important for the oxidation SO_2.

Furthermore, comparisons between satellite-derived data sets (e. g., Pohl et al., 2024) or cross-validations between models and observations (e. g., Quaglia et al., 2023; Sellitto et al., 2023) reveal inconsistencies. The primary source of these discrepancies in satellite observations stems from necessary assumptions regarding aerosol size and composition which introduce systematic uncertainties in the satellite-derived data sets. The recently developed Scanning Imaging Absorption Spectrometer for Atmospheric Chartography aerosol particle size distribution (SCIAMACHY v2.0 PSD) algorithm that provides global vertical profiles of aerosol size and extinction coefficients (Pohl et al., 2024), assumes a fixed particle number density (N) profile, representative for background aerosol conditions. This assumption becomes questionable after sulfur-rich volcanic eruptions, which can significantly enlarge N and introduce additional uncertainties in the retrieved optical aerosol properties.

In order to enhance the confidence in both the SCIAMACHY retrievals and GCM simulations, this study compares aerosol optical properties retrieved from SCIAMACHY with simulations from the middle atmosphere GCM MAECHAM5-HAM, following the Sarychev (2009) and Manam (2004/05) eruptions. This comparison follows a synergistic approach: satellite observations are used to assess the performance of the GCM with coupled aerosol microphysics and to improve the process understanding of particle size and plume transport, while the model results support the evaluation of the SCIAMACHY-retrieved aerosol properties. We demonstrate the robustness of the SCIAMACHY retrievals in the aftermath of volcanic eruptions, despite the assumption of a fixed aerosol number density profile.

The SCIAMACHY retrieval algorithm and the MAECHAM5-HAM model are described in Sect. 2. Comparisons following the Sarychev (2009) and Manam (2004/05) eruptions are presented in Sect. 3. Section 4 discusses the impact of assumptions in the satellite retrieval, model configuration, and model input data. Conclusions are provided in Sect. 5.

2 Methods

2.1 SCIAMACHY v2.0 aerosol PSD retrieval

The stratospheric aerosol optical properties are retrieved from SCIAMACHY limb radiances using a non-linear regularized inversion approach. The retrieval is described in detail in Pohl et al. (2024), a brief summary is provided here. Radiances

https://doi.org/10.5194/egusphere-2026-578
Preprint. Discussion started: 6 February 2026

from six wavebands with center wavelengths between 750 nm and 1300 nm are used. The retrieval assumes spherical particles composed of 75 % sulfuric acid and 25 % water at 0 % relative humidity. Their PSD is described by a monomodal lognormal distribution. The median radius and the geometric standard deviation are retrieved in 3.3 km steps between 18 and 35 km altitude, assuming a fixed number density profile (N). From these parameters, aerosol extinction coefficients (Ext) and effective radii (r_{eff}) are calculated. The spatial resolution of aerosol properties depends on the SCIAMACHY observations and is 2.6 km (vertical) and 240 x 400 km^2 (horizontal). For simplicity, this retrieval is refered to as SCIA PSD.

For the discussion in Sect. 4.1, we also present results from two additional SCIAMACHY retrieval versions. The first, SCIA PSD N_{WY}, uses a different number density profile N_{WY} within the SCIAMACHY v2.0 aerosol PSD retrieval. This profile is based on balloon-borne measurements over Wyoming and is shown in Fig. 4(c) in Pohl et al. (2024) by a red line. The second, SCIAMACHY v3.0 aerosol extinction retrieval (SCIA Ext), directly retrieves the aerosol extinction coefficients from SCIAMACHY radiances. The retrieval algorithm is described in Sofieva et al. (2024).

2.2 MAECHAM5-HAM simulations

The simulations for this study were performed with MAECHAM5 (Giorgetta et al., 2006). MAECHAM5 was applied with spectral truncation at wave-number 63 (T63), corresponding to a grid size of about $1.8° \times 1.8°$, and 95 vertical layers extending to the model top at 0.01 hPa. The model solves prognostic equations for temperature, surface pressure, vorticity, divergence, and phases of water. A land-sea mask, sea surface temperature (SST), and sea ice are prescribed and are set to climatological values (Hurrell et al., 2008), averaged over the period from 1950 to 2000. To achieve realistic wind and transport conditions during the course of the simulation, the large wave numbers of the model were nudged to the latest ECMWF reanalysis data (ERA5) (Hersbach et al., 2020). However, this may suppress the impact of aerosol heating on aerosol transport because the nudging data does not include short-term dynamic changes caused by aerosol heating within the volcanic cloud. Nevertheless, the nudging avoids the fast transport of sulfate to the poles due to the strong stratospheric meridional transport.

The prognostic modal aerosol microphysical Hamburg Aerosol Model (HAM, Stier et al. (2005)) is interactively coupled to MAECHAM5 (MAECHAM5-HAM, ECHAM thereafter). HAM calculates the formation of sulfate aerosols including nucleation, accumulation, condensation and coagulation, and their removal processes by sedimentation and deposition. We prescribe reactive gases (e. g., ozone, nitrogen oxides, hydroxyl radical–OH) and photolysis rates of carbonyl sulfide (OCS), SO_2, H_2SO_4, SO_3, and ozone on a monthly average basis. HAM uses four log-normal modes to describe the aerosol size distribution: nucleation, Aitken, accumulation and coarse mode. The modes are defined by the number median radius ($r_{\mathrm{g,i}}$) and the geometric standard deviation ($\sigma_{\mathrm{g,i}}$): nucleation mode $r_{\mathrm{g}} < 0.005\,\mu\mathrm{m}$, Aitken mode $0.005\,\mu\mathrm{m} < r_{\mathrm{g}} < 0.05\,\mu\mathrm{m}$, accumulation mode $0.05\,\mu\mathrm{m} < r_{\mathrm{g}} < 0.2\,\mu\mathrm{m}$, coarse mode $r_{\mathrm{g}} > 0.2\,\mu\mathrm{m}$.

HAM has been adapted to stratospheric conditions: a stratospheric chemistry for SO_2 oxidation is used above the tropopause (Hommel et al., 2011). Nucleation processes are simulated following Määttänen et al. (2018). The parameterization is valid for low stratospheric temperatures and high SO_2 concentrations in a volcanic cloud, which makes particle collision important. The geometric standard deviation of the mode bins (σ) differs from the original tropospheric setup (Kokkola et al., 2008; Niemeier et al., 2009). Changing the geometric standard deviations of a mode can be used to mimic the special condition in a

https://doi.org/10.5194/egusphere-2026-578
Preprint. Discussion started: 6 February 2026

Table 1. Eruption characteristics of Manam (2004/2005), Kasatochi (2008), and Sarychev (2009) eruptions as used in the simulations.

	Date / Time	Duration	SO_2 mass [Gg]	Altitude range [km]	reference
Manam					
1	24.10.2004 10 UTC	5 hours	13	15.7 - 17.8	volcano.si.edu
2	31.10.2004 10 UTC	5 hours	13	14.5 - 16.8	volcano.si.edu
3	11.11.2004 10 UTC	5 hours	8	10 - 12.4	volcano.si.edu
4	24.11.2004 10 UTC	5 hours	111	15.7 - 17.8	volcano.si.edu
5	20.12.2004 10 UTC	5 hours	38	14.5 - 16.8	volcano.si.edu
6	27.01.2005 14 UTC	5 hours	140	16.2 - 18.5	Neely III and Schmidt (2016)
Kasatochi					
1	7.8.2008 0 UTC	6 hours	1700	12.5 - 15.5	Karagulian et al. (2010), Waythomas et al. (2010), volcano.si.edu
Sarychev					
1	14.6.2009 0 UTC	12 hours	35	17 - 20	Lurton et al. (2018, and references therein), Rybin et al. (2011)
2	16.6.2009 0 UTC	24 hours	665	13 - 16	Lurton et al. (2018, and references therein), Rybin et al. (2011)

volcanic cloud. Kokkola et al. (2008) determined the particle number distribution of sulfur for different SO_2 concentrations and demonstrated how the results depend on the mode setup. Based on these results, we decided to use only three modes: nucleation, Aitken, and accumulation mode, with σ = 1.59 for our simulations. We omitted the coarse mode, similar to previous studies of stronger volcanic eruptions (Niemeier et al., 2009, 2021), which represents the particle size distribution after volcanic eruptions much better than the setup with four modes. As the SO_2 concentration after the eruptions in this study is closer to the SO_2 load in stratospheric aerosol intervention studies, we also tested the mode distribution used in Niemeier and Timmreck (2015). Their distribution included an additional coarse mode width $\sigma = 1.2$.

For our comparison study we performed simulations of the different phases of the Manam eruption (October 2004 until January 2005) and Sarychev eruptions (June 2009). To obtain more realistic background aerosol concentrations and size, we included the Kasatochi eruption (August 2008) in ECHAM. Details of the eruption characteristics are given in Table 1. We calculated the eruption rate based on the given SO_2 mass and eruption duration, then injected the SO_2 equally into five levels within the given altitude range.

https://doi.org/10.5194/egusphere-2026-578
Preprint. Discussion started: 6 February 2026

3 Results

Retrievals from SCIAMACHY are compared with simulations from the ECHAM model for the Sarychev (2009) and Manam (2004/05) eruptions. The results are zonally averaged over 10 d periods. Due to different vertical grid sampling intervals (0.5 km in the case of ECHAM, 3.7 km in the case of SCIAMACHY), ECHAM data are averaged in the altitude range $\pm$ 1.7 km around each SCIAMACHY observation level for improved comparability between ECHAM and SCIAMACHY. In the Discussion (Sect. 4.2), where the ECHAM parameter study is conducted, ECHAM data are presented on the original vertical grid.

3.1 Sarychev eruption 2009

The evolution of Ext and r_{reff} simulated by ECHAM and observed by SCIAMACHY after the 2009 Sarychev eruption is shown in Figs. 1 and 2. Both simulation and observation exhibit strong agreement in the volcanic plume dispersion and particle size distribution. The main plume reaches 21.5 km altitude and drifts towards the equator, similarly seen by ECHAM and SCIAMACHY. The simulated and observed maximum values of Ext are also in agreement. With SCIAMACHY, a slightly longer lifetime of the aerosol plume is observed than with ECHAM (Fig. 1).

Following the eruption, ECHAM simulates a pronounced decrease in aerosol size to $r_{\mathrm{eff}} = 0.11\,\mu\mathrm{m}$, driven by nucleation from elevated SO_2 and H_2SO_4 gas concentrations. In contrast, SCIAMACHY retrievals indicate a weaker decline (Fig. 2). Over time, aerosols grow to twice their original size ($r_{\mathrm{eff}} = 0.22\,\mu\mathrm{m}$) due to condensation and coagulation processes. The SCIAMACHY retrieval shows a similar increase in r_{reff} as the ECHAM simulations. Remarkable is the agreement of the aerosol size reduction observed by SCIAMACHY and simulated by ECHAM at the upper edge of the aerosol plume in 21.7 km altitude (Fig. 2 b,e).

A small part of the volcanic aerosol plume is lifted to higher altitudes over the Himalayas immediately after injection and is carried towards the polar regions by the easterly wind (not shown). This leads to an increase of Ext and r_{reff} at latitudes north of 50 °N as seen by ECHAM and SCIAMACHY (Figs. 1 and 2).

3.2 Manam eruption 2004/2005

Figures 3 and 4 show the comparison of Ext and r_{eff} simulated by ECHAM and observed by SCIAMACHY after the Manam eruptions 2004/2005. The layout of the figures is analogous to the figures of the Sarychev eruption (Figs. 1 and 2). Again, the vertical grids of the ECHAM and SCIAMACHY data are harmonized by averaging ECHAM data within $\pm$ 1.7 km around each SCIAMACHY observation level. For the lowest level ($z = 18.4$ km), averaging is restricted to 18.4 – 20.1 km to exclude tropospheric contributions. Additional white filled circles are included in the figures that form vertically aligned lines. They indicate the latitudes and times of SAGE II measurements which are used later in the Discussion (Sect. 4) for comparison purposes.

SCIAMACHY observations and ECHAM simulations show a good overall agreement in Ext (Fig. 3). Most of the plume is located in the equatorial region (20° S – 20° N) and extends vertically in time to approximately 23 km. Note that the additional plume observed by SCIAMACHY at 18.4 km and 40° S from April 2005 does not originate from the Manam eruption, but

https://doi.org/10.5194/egusphere-2026-578
Preprint. Discussion started: 6 February 2026

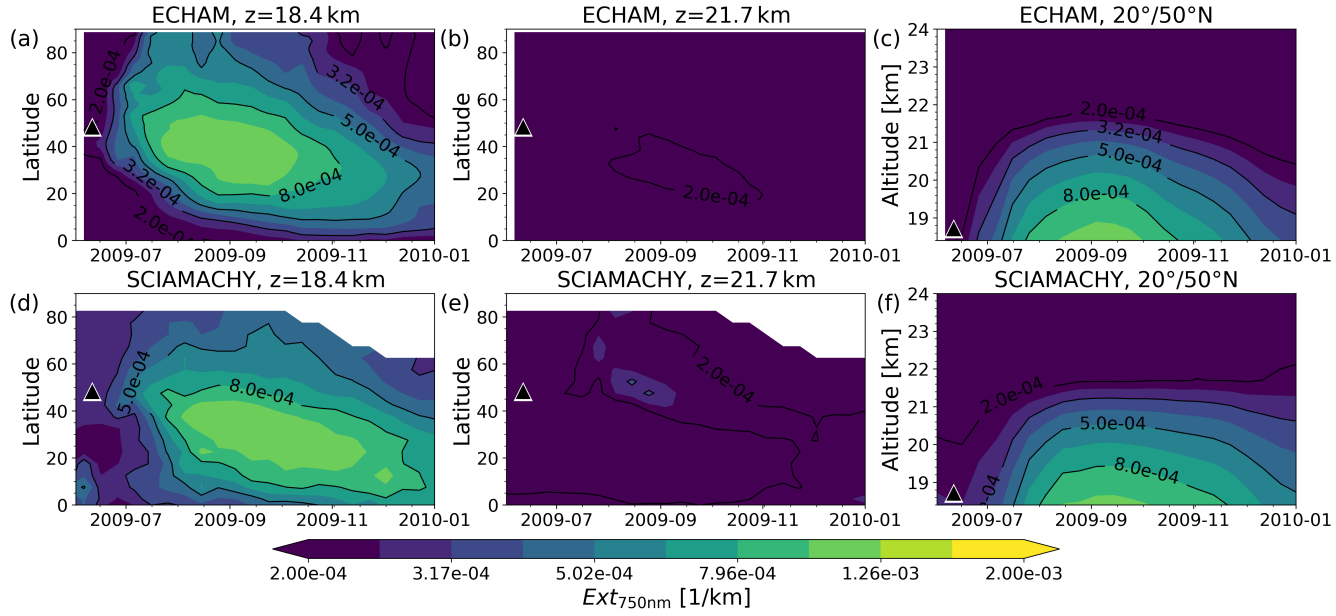

Figure 1. Sarychev eruption: Ten day zonal mean extinction coefficients at 750 nm from ECHAM (a-c) and SCIAMACHY (d-f) after the Sarychev eruption 2009. Simulations are vertically integrated on the SCIAMACHY altitude grid. Extinction coefficients in (c) and (f) are averaged in latitudinal bins between 20° and 50° N.

most likely from Australian bushfires. SCIAMACHY indicates higher Ext and a slight northward shift, while ECHAM plume extends farther south to about 40° S. In ECHAM, the plume exhibits faster vertical growth and descent, reaching its extinction maximum at 21.7 km in April, whereas SCIAMACHY observes the maximum in August. We will discuss possible reasons for the different simulated plume dispersion in Section 4.2.

The effective radii observed by SCIAMACHY and simulated by ECHAM exhibit distinct differences (Fig. 4). Prior to the eruption in January 2005, ECHAM simulations yield lower background values in r_{eff} at 18.4 km than SCIAMACHY, despite including the eruptions at the end of 2004. At 21.7 km, simulated r_{eff} is larger than observed by SCIAMACHY. After the eruption, ECHAM maintains small plume aerosol sizes for about one month at lower altitudes, whereas SCIAMACHY records an immediate increase. A possible explanation for this discrepancy can be a divergent background aerosol concentration at the time of the eruption. Background aerosols can act as condensation nuclei for injected sulfur. This process may cause the relative fast particle growth in the observation.

Above 21 km, SCIAMACHY reveals a pronounced decrease in r_{eff} for two months (Fig. 4f). This radius minimum is not visible in ECHAM simulations. However, using the original ECHAM grid and adjusting the injection altitude reproduces this characteristic (Sect. 4.2.2), confirming its physical origin rather than indicating a retrieval artifact in SCIAMACHY. With time, aerosol sizes increase consistently in ECHAM and SCIAMACHY, exceeding 0.19 µm in ECHAM in 21.7 km altitude, while SCIAMACHY detects smaller values with maximum sizes about 0.18 µm in 18.4 km altitude.

https://doi.org/10.5194/egusphere-2026-578
Preprint. Discussion started: 6 February 2026

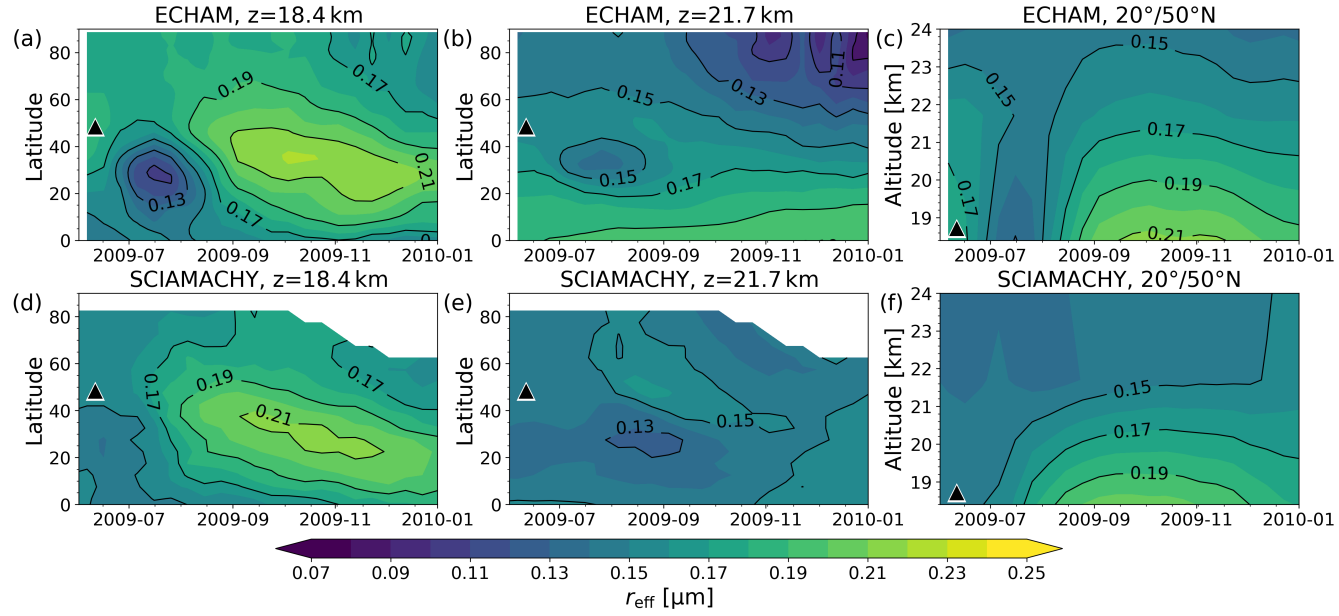

Figure 2. Sarychev eruption: Ten day zonal mean effective radius from ECHAM (a-c) and SCIAMACHY (d-f) after the Sarychev eruption 2009. Simulations are vertically integrated on the SCIAMACHY altitude grid. Extinction coefficients in (c) and (f) are averaged in latitudinal bins between 20° and 50° N.

4 Discussion

4.1 Assumption of a fixed number density profile

The SCIAMACHY v2.0 aerosol PSD algorithm assumes a number density profile to retrieve the median radius and the geometric standard deviation. This number density is fixed and representative of background aerosol conditions, which does not reflect the stratospheric aerosol level following volcanic eruptions. As a result, the retrieved size parameters (median radius and geometric standard deviation) and derived quantities such as Ext and r_{eff} may be subject to larger uncertainties. To assess the impact of the assumed number density profile on the SCIAMACHY retrievals, the evolution of stratospheric aerosols following the Manam eruptions of 2004/2005 is investigated. This period was chosen due to the availability of independent SAGE II data for comparison.

Figures 5 and 6 present Ext and r_{eff} of SAGE II, ECHAM, and SCIAMACHY, respectively. Data are zonally averaged within three time intervals 6 - 17 March, 19 April - 5 May, and 25 June - 13 July 2005, corresponding to periods with available SAGE II observations (white lines indicated in Figs. 3 and 4). SAGE II Ext (first row in Fig. 5) was derived using the SAGE II version 7.0 algorithm (Damadeo et al., 2013), SAGE II r_{eff} (first row in Fig. 6) was derived from the 525/1020 nm extinction ratio and assuming a geometric standard deviation of $\sigma_{\mathrm{g}} = 1.5$ (Pohl et al., 2024). In addition to the ECHAM simulations (second row in Figs. 5 and 6), and the SCIAMACHY v2.0 aerosol PSD retrievals (third row), two further SCIAMACHY-

https://doi.org/10.5194/egusphere-2026-578
Preprint. Discussion started: 6 February 2026

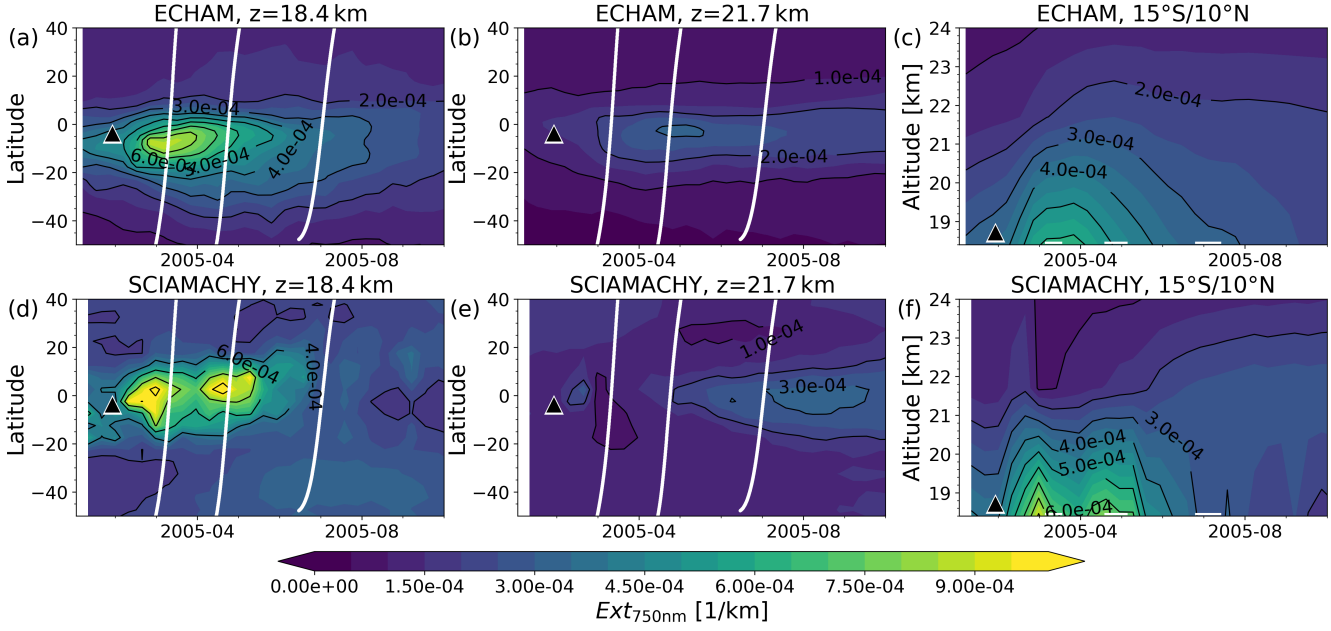

Figure 3. Manam eruption: Ten day zonal mean extinction coefficients at 750 nm from ECHAM (a-c) and SCIAMACHY (d-f) after the Manam eruptions 2004/2005. Simulations are vertically integrated on the SCIAMACHY altitude grid. Extinction coefficients in (c) and (f) are averaged in latitudinal bins between 15° S and 10° N. Filled white circles which form vertically aligned white lines indicate latitudes and times of SAGE II measurements.

derived data sets are included in the comparison. The first data set (SCIA PSD N_{WY}, fourth row) has been generated using the same SCIAMACHY v2.0 aerosol PSD retrieval algorithm, but using a modified number density profile. This profile is based on balloon-borne measurements over Wyoming (red line in Fig. 4 c) in Pohl et al. (2024). The second data set (SCIA Ext, fifth row in Fig. 5) consists of Ext retrieved directly from SCIAMACHY observations (SCIAMACHY v3.0 aerosol extinction retrieval (Sofieva et al., 2024)).

The best agreement in Ext is observed between SAGE II and the SCIAMACHY v2.0 aerosol PSD retrieval. Modifying the number density profile in the SCIAMACHY retrieval only affects the magnitude of Ext, while its spatial distribution remains unchanged. Among the three SCIAMACHY datasets, direct Ext retrieval (SCIA Ext, Fig. 5 m-o) yields the lowest values. This comparison demonstrates that SCIAMACHY PSD retrieval provides the most realistic Ext results, despite the assumption of a fixed number density profile. Additionally, the comparison with SAGE II confirms a slight underestimation of ECHAM-simulated Ext data. Furthermore, ECHAM places the plume center and extent too far south during the first two time periods (Fig. 5 d,e), whereas in the third period (Fig. 5 f) the Ext magnitude agrees more closely with SAGE than with SCIAMACHY.

SAGE II, SCIAMACHY, and ECHAM show pronounced differences in both the spatial distribution and the magnitude of r_{eff} (Fig. 6). However, caution is required when interpreting these discrepancies, as SAGE II r_{eff} is a secondary retrieved product (retrieval from retrieved aerosol extinction coefficients). This indirect retrieval might introduce greater uncertainties into the

https://doi.org/10.5194/egusphere-2026-578
Preprint. Discussion started: 6 February 2026

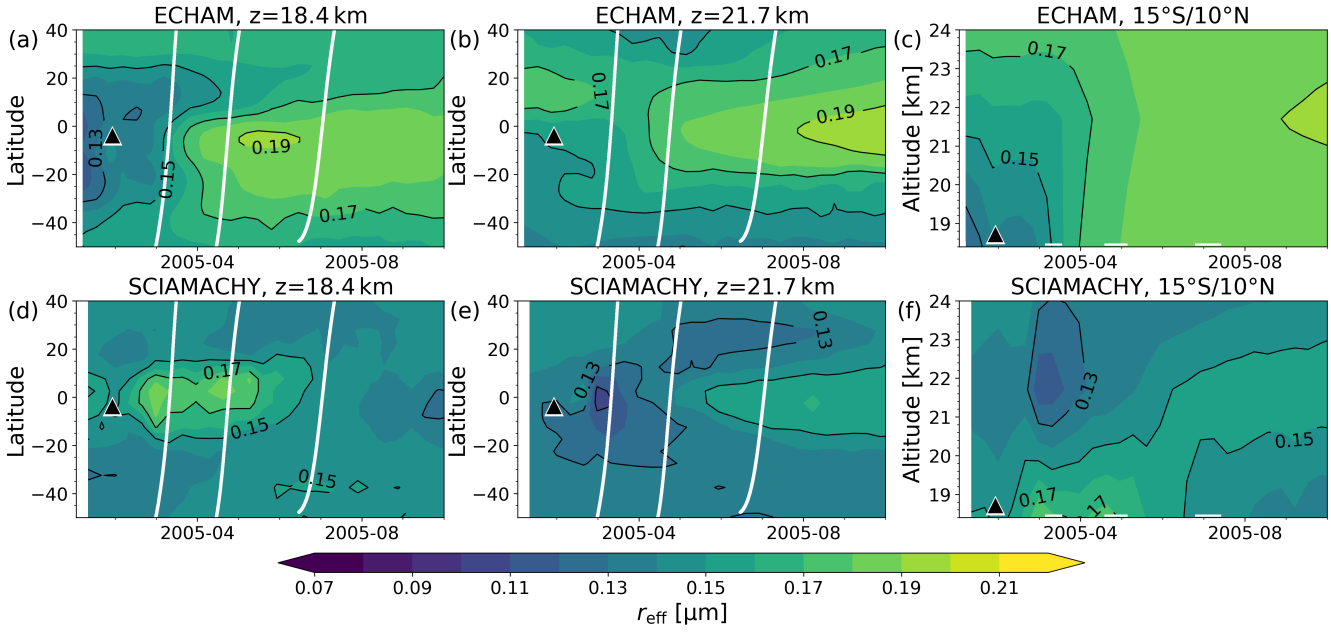

Figure 4. Manam eruption: Ten day zonal mean effective radius from ECHAM (a-c) and SCIAMACHY (d-f) after the Manam eruptions 2004/2005. Simulations are vertically integrated on the SCIAMACHY altitude grid. Extinction coefficients in (c) and (f) are averaged in latitudinal bins between 15° S and 10° N. Filled white circles which form vertically aligned white lines indicate latitudes and times of SAGE II measurements.

retrieved product, limiting the comparability of SAGE II r_{eff} with other datasets and partially account for the discrepancies in r_{eff} retrieved from SCIAMACHY and SAGE II.

In March (Fig. 6, first column), below 20 km in the southern tropics, aerosol growth in the plume core observed by SCIA-
215 MACHY is confirmed by SAGE II observations. However, SAGE reports larger particles ($r_{\mathrm{eff}} > 0.21$ µm) than SCIAMACHY ($r_{\mathrm{eff}} > 0.16$ µm). Around the plume core, all three datasets (SAGE II, SCIAMACHY, and ECHAM) show a decrease in aerosol size relative to background conditions, likely due to nucleation processes. This is evident as local minima adjacent to or above the plume center, although their prominences vary across data sets. An equatorial minimum in r_{eff} near 22 km altitude appears consistently in both SAGE II and SCIAMACHY. ECHAM also reproduces this feature, albeit at a slightly lower altitude. This
220 feature can be only visualized on the model's high-resolution vertical grid rather than on the coarser grid (see Fig. 8a).

Over time (Fig. 6, second column), all data sets indicate a volcanic aerosol size growth. However, discrepancies emerge in summer (Fig. 6, third column): while SAGE II indicates a large-scale reduction in r_{eff}, ECHAM simulates continued growth. SCIAMACHY shows a size change dependent on the number density, but particles remain larger than background levels.

Such discrepancies in particle sizes between observations and model simulations have been reported previously (e. g., Wrana
225 et al. (2023)): SAGE III retrievals showed persistently small aerosol sizes for months following the Ambae, Ulawun, and La Soufrière eruptions. Although ECHAM simulated an initial decrease in aerosol size after Ulawun, the simulations showed

https://doi.org/10.5194/egusphere-2026-578
Preprint. Discussion started: 6 February 2026

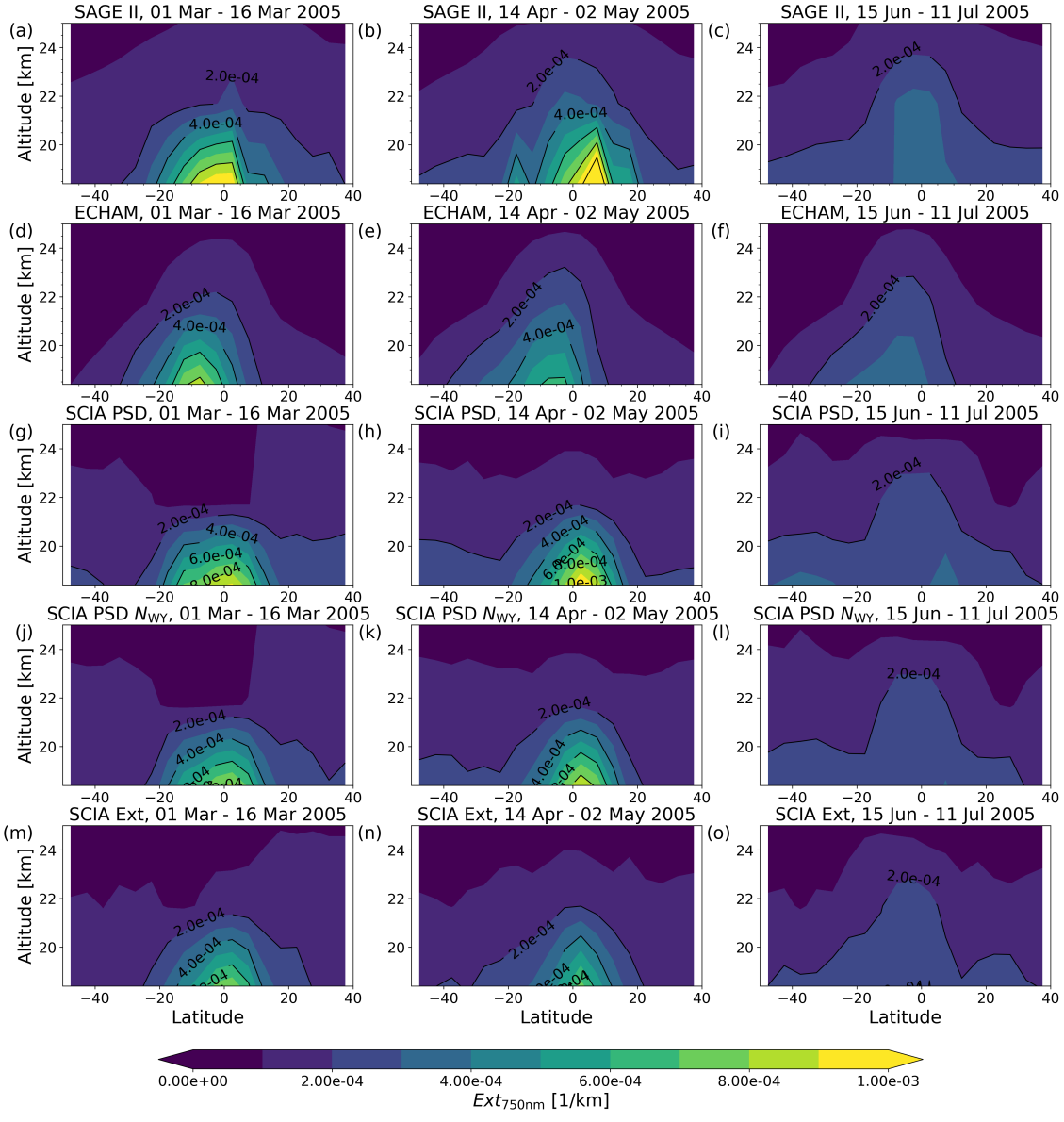

Figure 5. Manam eruption: Zonal mean extinction coefficients at 750 nm averaged between 1 - 16 March (left column), 14 April - 2 May (middle column), and 15 June - 11 July (right column) after the Manam eruptions 2004/2005. Specified time limits correspond to the positions of the start and end time of white lines in Fig. 3. Extinction coefficients are from SAGE II (a-c), ECHAM (d-f), the SCIAMACHY v2.0 PSD retrieval (g-i), the SCIAMACHY PSD retrieval using the number density profile based on balloon-borne measurements over Wyoming (j-l), and SCIAMACHY v3.0 Ext retrieval (m-o).

particle growth after two months. These discrepancies highlight persistent challenges in accurately representing the aerosol size after volcanic eruptions.

https://doi.org/10.5194/egusphere-2026-578
Preprint. Discussion started: 6 February 2026

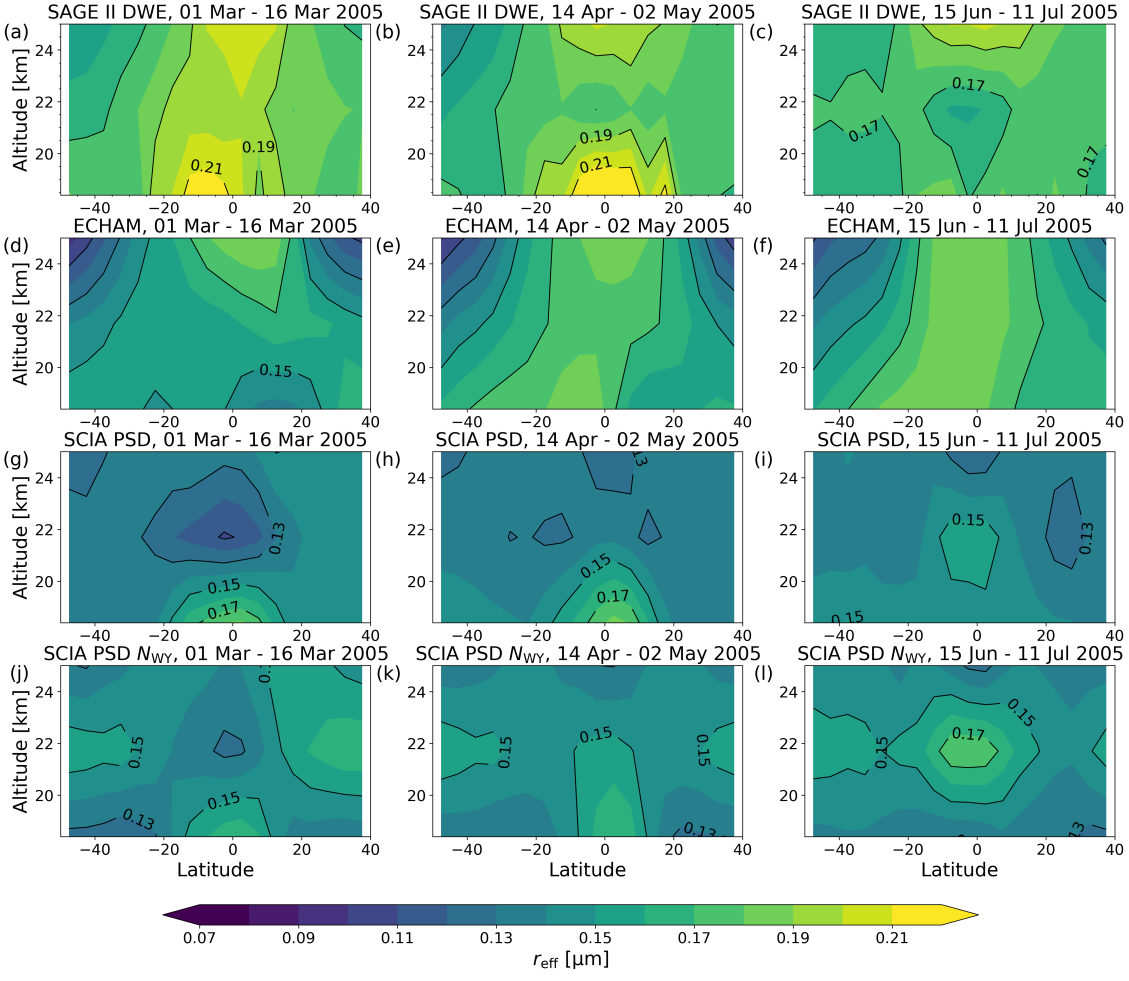

Figure 6. Manam eruption: Zonal mean effective radius in the same time frames as in Fig. 5 after the Manam eruptions 2004/2005. The effective radius is from SAGE II (a-c), ECHAM (d-f), the SCIAMACHY PSD retrieval (g-i), and the SCIAMACHY PSD retrieval using the number density profile based on balloon-borne measurements over Wyoming (j-l).

4.2 ECHAM parameter study

In order to obtain model results closest to the satellite retrieval data, we modified several parameters in ECHAM and introduced nudging to the ERA5 reanalysis data. We also adjusted the background and initial data for the simulations and performed different studies with changing injection areas. Results of our test simulations are shown in Figs. 7 to 10.

4.2.1 Nudging

As discussed in several papers (e. g., Niemeier et al., 2009; Marshall et al., 2019; Quaglia et al., 2023), the simulated meridional transport towards the poles in the lower stratosphere in ECHAM is stronger than observed. One reason for this is the relatively

https://doi.org/10.5194/egusphere-2026-578
Preprint. Discussion started: 6 February 2026

low vertical advection in the tropical pipe (Niemeier et al., 2021), which results in a weak subtropical transport barrier and less blocking of the meridional transport out of the tropics in the lower branch of the Brewer-Dobson circulation. The nudging of the model towards the ERA5 data (see Sect. 2.2) brings the model closer to the observed distribution of volcanic aerosols (Malinina et al., 2021). This nudging, and with it the constrained transport of the aerosols, is one important reason for the close consistency of the model results and the observations for the Sarychev eruption. However, we see differences in the transport in the Manam comparisons. Figures 3 and 5 show the center of the volcanic cloud slightly further north in the observations than in the simulations.

Sulfate aerosols interact with both solar and terrestrial radiation. They scatter shortwave radiation, resulting in lower surface temperatures. At the same time, the aerosols absorb near-infrared and infrared radiation. This has two consequences: a positive temperature anomaly in the stratospheric aerosol layer, and consequent changes in stratospheric dynamics. In simulations with artificial sulfur injections, the quasi-biennial oscillation (QBO) broke down (Aquila et al., 2014; Niemeier and Schmidt, 2017).

However, the ERA5 data does not include sulfate aerosols following volcanic eruptions, nor does it include the heating of these aerosols. The nudging data can only reflect the impact of aerosol heating on stratospheric dynamics through data assimilation. Therefore one reason for the different transport might be that the nudging data override the impacts of sulfate heating simulated in the model. In a simulation without nudging, we could demonstrate that more aerosols would cross the equator, although still fewer than in the observations (not shown). Therefore, we only present nudged model results.

4.2.2 Vertical injection profile

Axebrink et al. (2024) demonstrate the importance of the initial injection profile in determining the outcome of a model simulation of the Sarychev eruption. Similar to Axebrink et al. (2024), we observed a clear dependence of the final aerosol distribution on the injection altitude. However, our comparison is limited to the upper part of the volcanic plume (>18 km). We achieved the best agreement with SCIAMACHY using a simple vertical profile with equal injection into five vertical grid points. The injection altitude varied depending on the eruption (see Tab. 1). However, it is important to take a closer look at the details of how the eruption unfolded. For the Sarychev eruption, for example, we had to include the smaller eruption that occurred two days prior to the main eruption on 14 June 2009, in order to accurately model the eastward transport of the volcanic cloud as observed.

For the Manam comparison, we also tested different injection altitudes. The first row in Figs. 7 and 8 shows results for Manam 6, as listed in Tab. 1. The second and third row show results with injection altitudes increased by 1.5 km and 3.0 km, respectively. As more aerosols were injected above 18 km altitude, Ext in the stratosphere increased with increasing injection altitude. The effective radii show a more complex behaviour. In the first weeks after the eruption, the particle radii decreased in the simulations with increased injection altitude. Increasing the injection altitude resulted in more sulfur in altitudes above 20 km, more nucleation, the formation of new small particles and consequently a smaller effective radius. We may conclude from these simulation that our injection altitude may be slightly too low.

https://doi.org/10.5194/egusphere-2026-578
Preprint. Discussion started: 6 February 2026

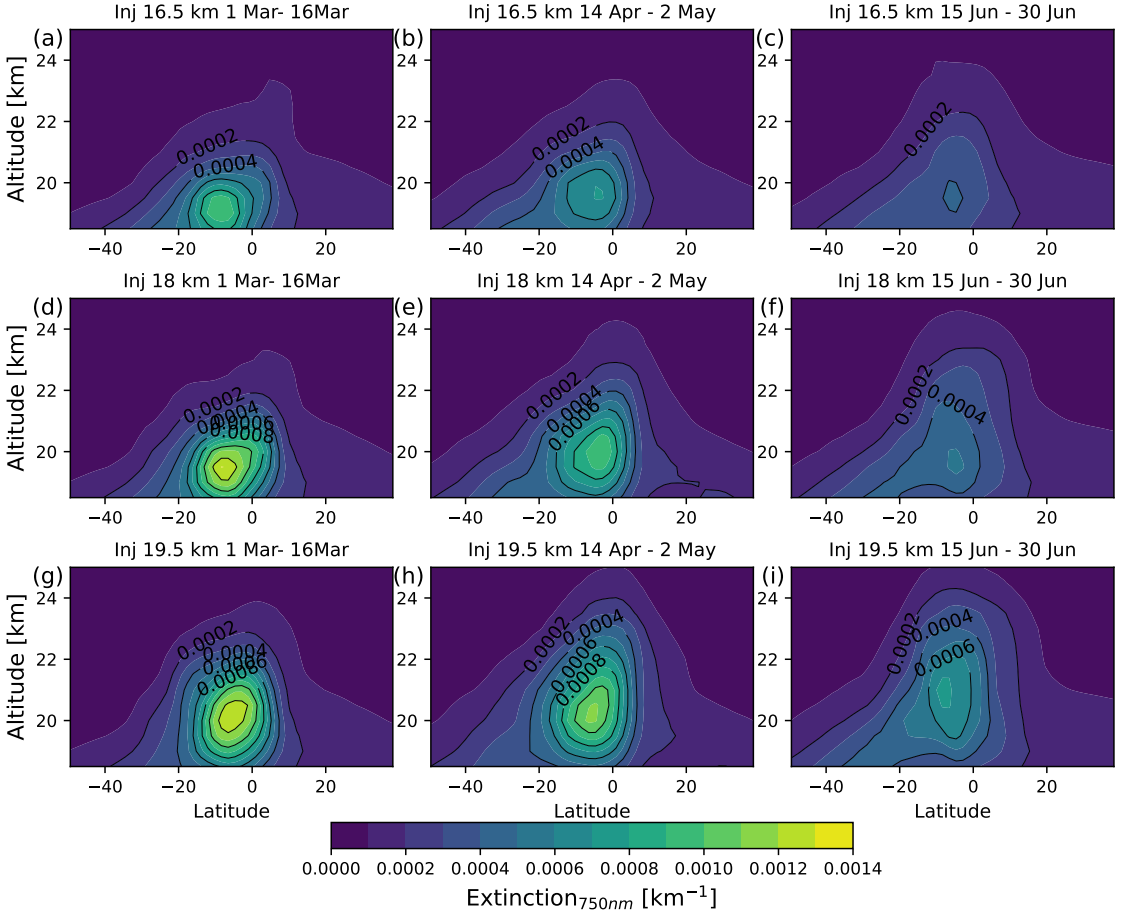

Figure 7. Manam eruption: Simulated zonal mean extinction coefficient at 750 nm in three scenarios, each with a different injection altitude. Results of the lowest injection altitude (first row), are similar to previously shown Manam results. The columns show three different time periods after the eruption of Manam.

4.2.3 Background aerosol

The simulations of the Sarychev and Manam eruption started from a 10 year long simulation with natural tropospheric sulfur
270 emissions - the background simulation. We included the series of small eruptions of the Manam volcano in 2004 and the 2008 Kasatochi eruption eight months before the Sarychev eruption in our simulations. Without these eruptions, the background aerosols show unrealistic low effective radii, especially before the Sarychey eruption (Fig. 10 (a) with and (e) without the Kasatochi eruption). The remaining sulfur aerosols from Kasatochi increased the particle size of the background conditions immediately before the Sarychev eruption from 0.12 to 0.18 µm around 30° N (Fig. 10 a).

https://doi.org/10.5194/egusphere-2026-578
Preprint. Discussion started: 6 February 2026

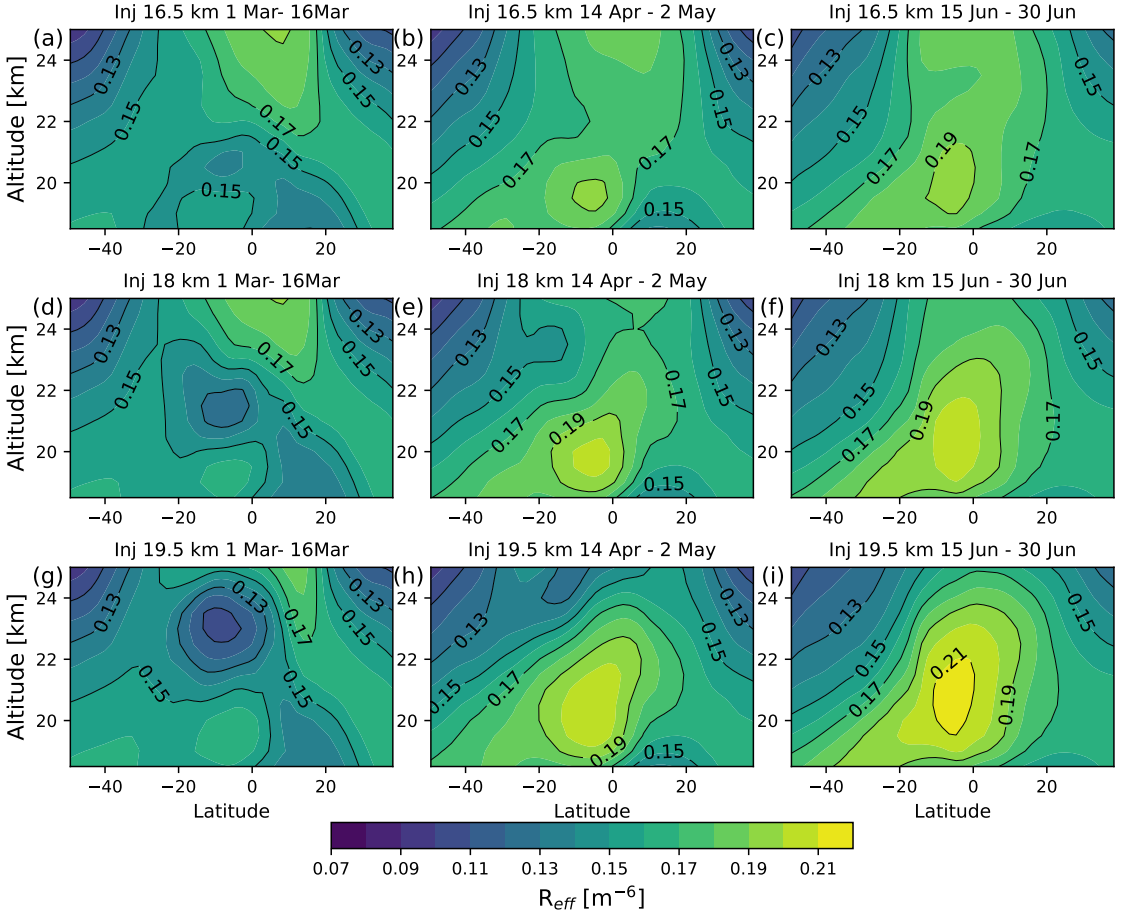

Figure 8. Manam eruption: Simulated zonal mean effective radius using the injection altitudes and time frames stated in Fig. 7.

Additionally, the Kasatochi eruption noticeably influences the evolution of the sulfate aerosols after the Sarychev eruption. Particle size and aerosol extinction coefficients are about 10 % larger within the volcanic plume when the Kasatochi eruption is included.

4.2.4 Horizontal injection area

Injecting the erupted SO_2 mass into one grid box, 1.8°x 1.8°, causes a relatively high SO_2 concentration. The subsequent oxidation of SO_2 to sulfuric acid depends on the concentration of the OH radical. Inside the volcanic cloud, the SO_2 concentration may be high enough to deplete OH. This results in reduced SO_2 oxidation and a longer lifetime of SO_2. Another process that can impact the formation of sulfate is volcanic ash. Zhu et al. (2020) simulated the uptake of SO_2 on ash, a process that effectively removes SO_2 from the volcanic cloud. They concluded that this process reduces the final sulfate concentration more effectively than OH depletion does. Both processes are not included in our simulations. Although we injected ash and SO_2

https://doi.org/10.5194/egusphere-2026-578
Preprint. Discussion started: 6 February 2026

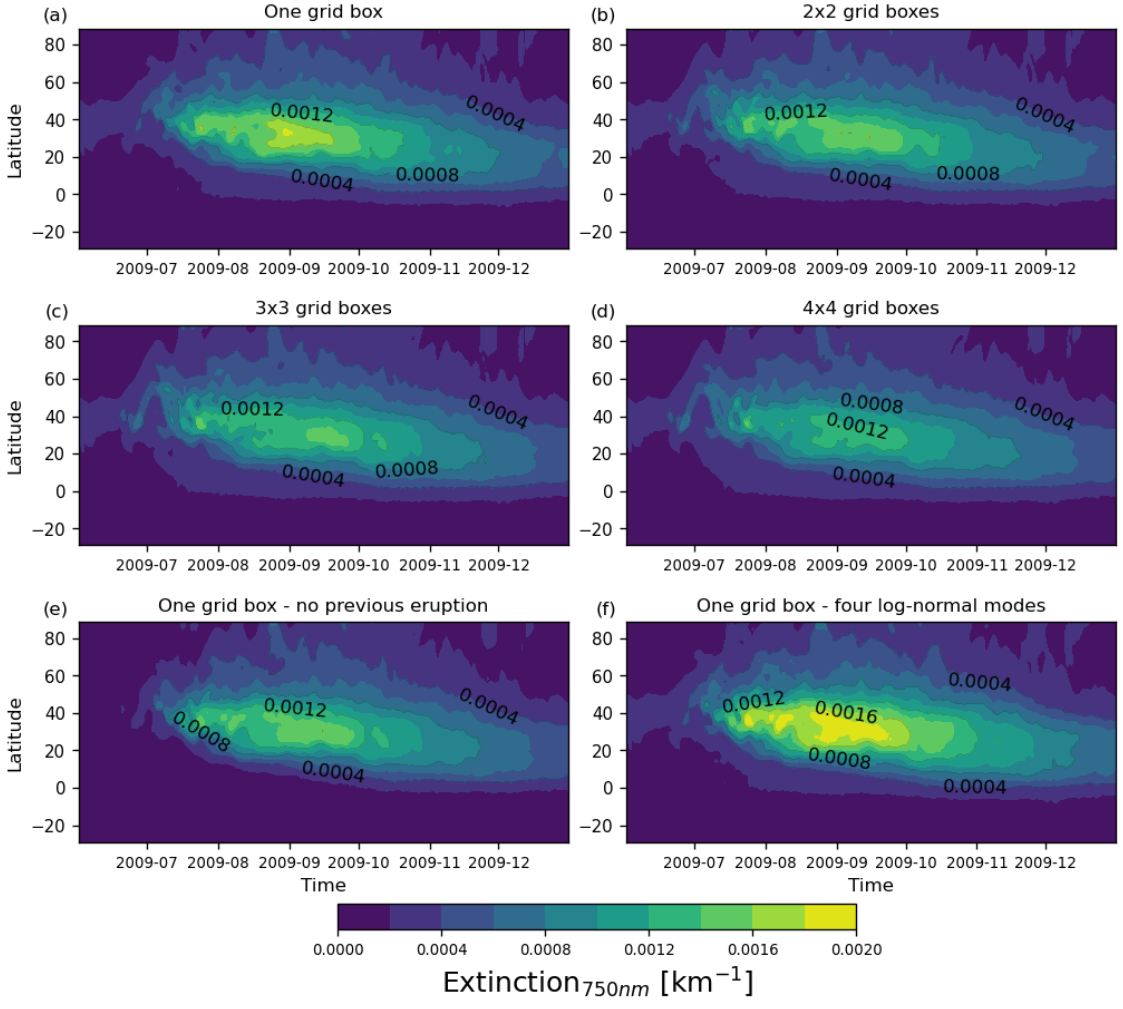

Figure 9. Sarychev eruption: Zonal mean aerosol extinction coefficient at 750 nm simulated with ECHAM using different injection scenarios. (a-d) Different injection area from 1x1 to 4x4 grid boxes. (e) Simulation without the 2008 Kasatochi eruption. (f) Four HAM size modes instead of three as assumed in previously simulations (Sect. 2.2).

285 together, they do not react with each other in the model. They only interact via dynamic changes due to the radiative heating of the ash (Niemeier et al., 2021), but the amount of ash in this study is too small to change the aerosol transport.

As the model is not coupled with full atmospheric chemistry, resulting in the above-mentioned deficiencies, we modulated the initial SO_2 injection. We increased the injection area from one grid box up to 4x4 grid boxes. This reduces the initial concentration of SO_2 per area and follows the strategy of several other studies (e. g., Tilmes et al., 2023; Sukhodolov et al., 290 2018). Figure 9 (a-d) shows the sulfate concentration at 18.5 km altitude for an injection into 1x1 to 4x4 grid boxes. Roughly, the aerosol extinction decreases by 10 % with each increase in the injection area, while the maximum effective radius decreases

https://doi.org/10.5194/egusphere-2026-578
Preprint. Discussion started: 6 February 2026

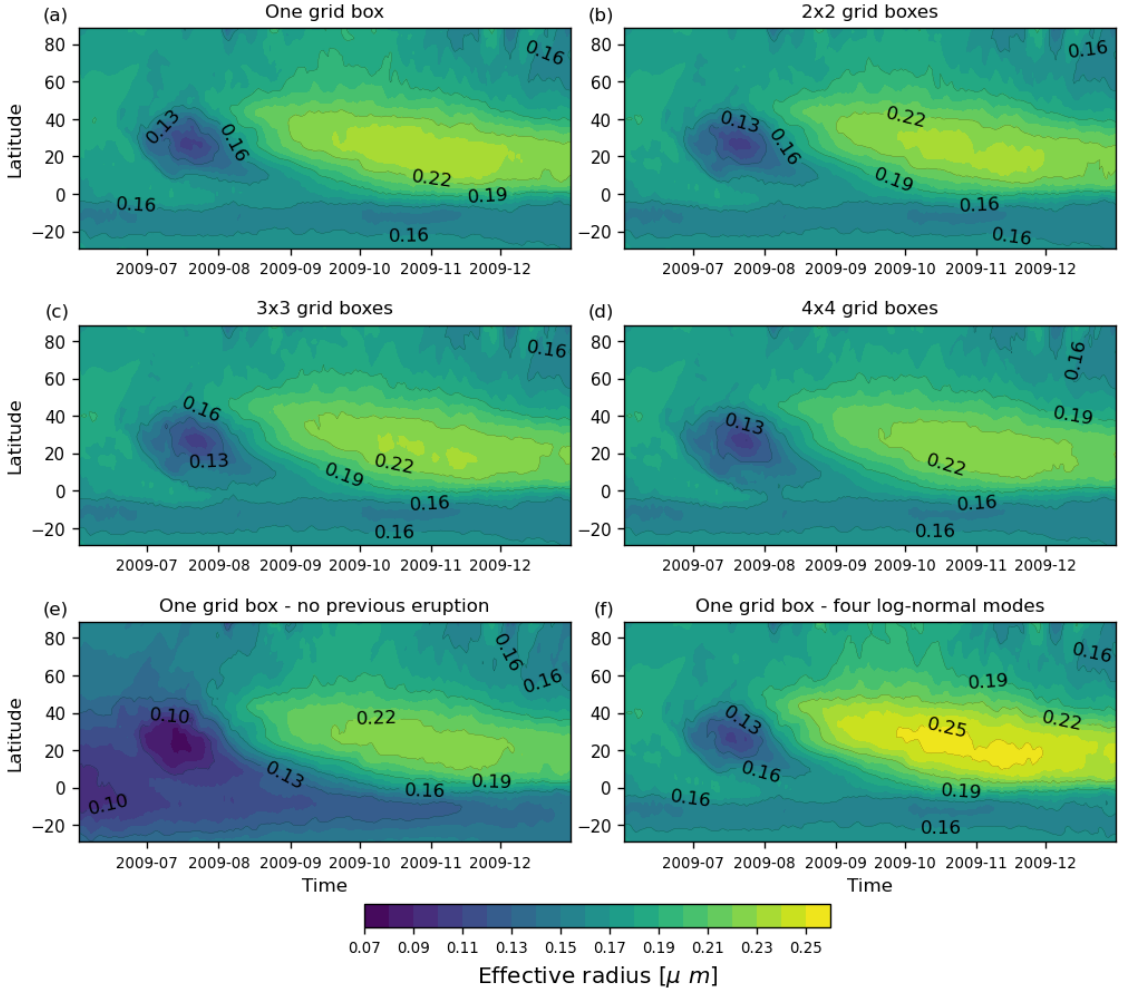

Figure 10. Sarychev eruption: Zonal mean effective radius simulated with ECHAM using different injection scenarios stated in Fig. 9.

by 10 % when the injection area increases from one grid box to four by four boxes (Fig. 10). The results of the larger injection area fitted best to the observations of SCIAMACHY. Therefore, we assume that increasing the injection area may help to overcome some model limitations. Following this comparison, we decided to use the 2x2 grid boxes as the injection area for the model to observation study.

4.3 Microphysical differences

ECHAM uses a modal size distribution of aerosols for its aerosol microphysics. Kokkola et al. (2008) have shown that the final particle size depends strongly on the details of this modal distribution, e. g., the number and width of modes. The original HAM setup with four modes (nucleation, Aitken, accumulation and coarse) was changed to a setup with three modes in this

https://doi.org/10.5194/egusphere-2026-578
Preprint. Discussion started: 6 February 2026

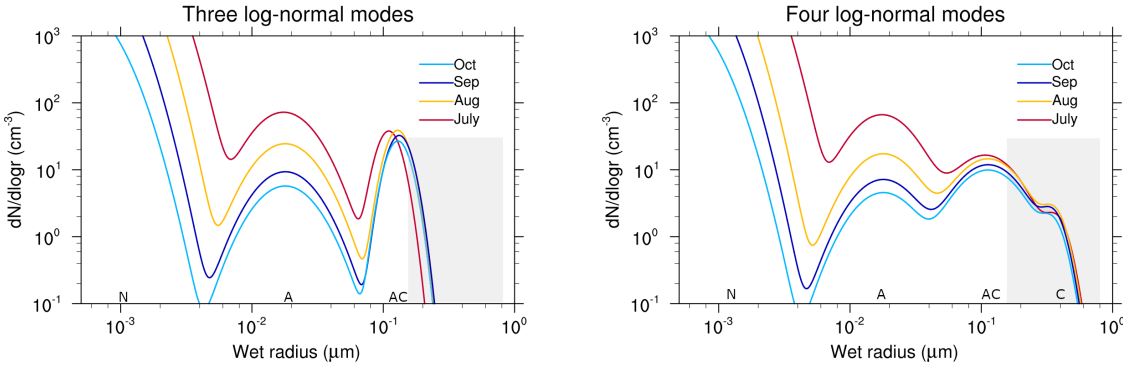

Figure 11. Simulated particle size distribution after the Sarychev eruption using three modes (a) and four modes (b) in the aerosol microphysics, respectively. Names of the modes from left to right are nucleation (N), Aitken (A), accumulation (AC) and coarse mode (C). Within the grey shaded areas backscattering is 70% of the maximum value (Laakso et al., 2022).

study (see Sect. 2.2). We also tested a four-mode setup for the Sarychev eruption, by increasing the σ of the accumulation mode to 1.59 and adding a coarse mode with a small width ($\sigma = 1.2$), as used in SAI studies (Niemeier and Schmidt, 2017). This results in slightly higher extinction (Fig. 9 f) and roughly 10 % larger effective radii (Fig. 10 f). In the early phase after the eruption, aerosol radii are similar in both simulations. Over time, the aerosols grow larger in the four-mode setup due to the wider accumulation mode and the additional coarse mode (Fig. 11). The transfer implies a decrease of the number density in the accumulation mode. Compared to SCIAMACHY retrievals, the three-mode setup of HAM yields better agreement (Fig. 2).

Although Laakso et al. (2022) used a continuous and idealized injection scenario, one additional key finding should be noted here: they pointed out that depending on the setting of the modes, gaps between the modes may occur. This may cause a lack of particles in a size range that is most effective for short-wave scattering (see the gray area in Fig. 11). This finding highlights the critical role of accurate mode representation in modal aerosol models.

5 Conclusions

This study compares aerosol optical properties, Ext and r_{eff}, retrieved from SCIAMACHY with ECHAM simulations following the Manam (2004/05) and Sarychev (2009) eruptions. The aim is to assess the performance of both the satellite retrieval and the model. Good agreement is found for Ext and r_{eff} after the Sarychev eruption, while larger discrepancies in plume dispersion and particle size appear after Manam.

Despite assuming a fixed N profile, the SCIAMACHY v2.0 PSD retrieval yields realistic vertical Ext profiles. Their absolute values agree better with SAGE II observations than those obtained using the SCIAMACHY approach that directly retrieves Ext. While modifications in the assumed N profile slightly affect the magnitude of Ext and r_{eff}, they have minimal impact on the vertical profile shape. The good agreement between SCIAMACHY v2.0 PSD retrievals and ECHAM simulations, particularly

https://doi.org/10.5194/egusphere-2026-578
Preprint. Discussion started: 6 February 2026

after the Sarychev eruption, demonstrates that SCIAMACHY v2.0 PSD provides reliable and useful aerosol size information. This makes SCIAMACHY v2.0 PSD a valuable data resource, especially given the limited availability of remote sensing data on aerosol size.

A model parameter study highlights the importance of using realistic injection profiles and background particle sizes in ECHAM for improving model–observation agreement. The results emphasize the crucial role of nudging in plume transport. Unfortunately, nudging can reduce self-induced dynamic effects of the volcanic aerosol plume. However, as the particle formation and growth are non-linear processes, many other factors influence the agreement between model simulations and satellite observations. Expanding the horizontal area of the injection in the model improves this agreement, compensating for limitations in the representation of sulfuric acid formation from OH. Accurate representation of the aerosol microphysical processes is also essential. In particular, the formation of small particles immediately after the eruption must be captured. This requires a nucleation scheme valid for the temperature range in the stratosphere, as well as the inclusion of collision processes under high sulfur conditions, as included in the nucleation parameterization after Määttänen et al. (2018). The correct setup of the aerosol size modes is very important, particularly the mode width. Otherwise the simulated particle size might be far too large. Bin microphysical models offer an alternative to modal approaches, as they respond more flexibly to varying sulfate concentrations without requiring assumptions about mode adaptation. However, they are a lot more computationally expensive, e. g., by a factor of three (Tilmes et al., 2023), which limits their applicability in comprehensive climate model simulation studies.

Our study highlights the importance of the details in the model setup parameters. It also demonstrates the robustness of the SCIAMACHY v2.0 PSD retrievals with respect to retrieval assumptions. Comparison studies like this are essential for building confidence in both satellite observations and model results. They improve our understanding of uncertainties in stratospheric aerosol intervention (SAI) simulations, which cannot be tested in nature and therefore depend entirely on modeling.

Data availability. Aerosol characteristics from the SCIAMACHY v2.0 aerosol PSD retrieval are available at https://www.iup.uni-bremen.de/DataRequest/ (last access: 24 Nov 2025). SAGE II v7.0 is available at https://doi.org/10.5067/ERBS/SAGEII/SOLAR_BINARY_L2-V7.0 (NASA/LARC/SD/ASDC, 2012), SAGE II aerosol effective radius derived from the 525/1020 nm extinction ratio will be made available on request.

Author contributions. CP was responsible for the satellite retrieval part, UN carried out the simulation part. CP and UN jointly performed the comparison, analysation, and writing. AR retrieved and provided the SCIAMACHY v3.0 Ext retrieval data. FW retrieved and provided the SAGE II aerosol effective radius derived from the 525/1020 nm extinction ratio. All authors contributed to the discussion and interpretation of the results.

Competing interests. At least one of the (co-)authors is a member of the editorial board of Atmospheric Measurement Techniques.

https://doi.org/10.5194/egusphere-2026-578
Preprint. Discussion started: 6 February 2026

Acknowledgements. This research has been funded in part by the Deutsche Forschungsgemeinschaft (DFG) via the Research Unit VolImpact (grant no. 398006378), by the ESA via the CREST and the STATISTICS project, and by the University and State of Bremen. HPC facilities of the IUP, University of Bremen, have been funded by DFG/FUGG grant nos. INST 144/379-1 and INST 144/493-1. MAECHAM5-HAM simulations have been performed at the computers of the German Climate Computing Center (DKRZ) under the account bm550.

https://doi.org/10.5194/egusphere-2026-578
Preprint. Discussion started: 6 February 2026

References

Aquila, V., Garfinkel, C. I., Newman, P., Oman, L. D. and Waugh, D. W. (2014). Modifications of the quasi-biennial oscillation by a geoengineering perturbation of the stratospheric aerosol layer, *Geophys. Res. Lett.* **41**: 1738–1744.

Aquila, V., Oman, L. D., Stolarski, R. S., Colarco, P. R. and Newman, P. A. (2012). Dispersion of the volcanic sulfate cloud from a mount pinatubo-like eruption, *Journal of Geophysical Research: Atmospheres* **117**(D6).
URL: *https://agupubs.onlinelibrary.wiley.com/doi/abs/10.1029/2011JD016968*

Axebrink, E., Sporre, M. K. and Friberg, J. (2024). High-resolution stratospheric volcanic so_2 injections in waccm, *EGUsphere* **2024**: 1–19.
URL: *https://egusphere.copernicus.org/preprints/2024/egusphere-2024-1448/*

Bernath, P., Boone, C., Pastorek, A., Cameron, D. and Lecours, M. (2023). Satellite characterization of global stratospheric sulfate aerosols released by tonga volcano, *Journal of Quantitative Spectroscopy and Radiative Transfer* **299**: 108520.

Boone, C. D., Bernath, P. F., Pastorek, A. and Lecours, M. (2024). Sulfate aerosol properties derived from combining coincident ace-fts and sage iii/iss measurements, *Journal of Quantitative Spectroscopy and Radiative Transfer* **312**: 108815.

Brenna, H., Kutterolf, S., Mills, M. J., Niemeier, U., Timmreck, C. and Krüger, K. (2021). Decadal disruption of the qbo by tropical volcanic supereruptions, *Geophysical Research Letters* **48**(5): e2020GL089687. e2020GL089687 2020GL089687.
URL: *https://agupubs.onlinelibrary.wiley.com/doi/abs/10.1029/2020GL089687*

Carn, S. A., Fioletov, V. E., McLinden, C. A., Li, C. and Krotkov, N. A. (2017). A decade of global volcanic so2 emissions measured from space, *Scientific reports* **7**(1): 44095.

Clyne, M., Lamarque, J.-F., Mills, M. J., Khodri, M., Ball, W., Bekki, S., Dhomse, S. S., Lebas, N., Mann, G., Marshall, L., Niemeier, U., Poulain, V., Robock, A., Rozanov, E., Schmidt, A., Stenke, A., Sukhodolov, T., Timmreck, C., Toohey, M., Tummon, F., Zanchettin, D., Zhu, Y. and Toon, O. B. (2021). Model physics and chemistry causing intermodel disagreement within the volmip-tambora interactive stratospheric aerosol ensemble, *Atmospheric Chemistry and Physics* **21**(5): 3317–3343.
URL: *https://acp.copernicus.org/articles/21/3317/2021/*

Damadeo, R. P., Zawodny, J. M., Thomason, L. W. and Iyer, N. (2013). Sage version 7.0 algorithm: application to sage ii, *Atmospheric Measurement Techniques* **6**(12): 3539–3561.

Eisinger, M., Marnas, F., Wallace, K., Kubota, T., Tomiyama, N., Ohno, Y., Tanaka, T., Tomita, E., Wehr, T. and Bernaerts, D. (2024). The EarthCARE mission: science data processing chain overview, *Atmospheric Measurement Techniques* **17**(2): 839–862.

English, J. M., Toon, O. and M.J., M. (2013). Microphysical simulations of large volcanic eruptions: Pinatubo and toba, *J. Geophys. Res. Atmos.* **118**: 1880–1895.

Giorgetta, M. A., Manzini, E., Roeckner, E., Esch, M. and Bengtsson, L. (2006). Climatology and forcing of the quasi–biennial oscillation in the MAECHAM5 model, *J. Climate* **19**: 3882–3901.

Haghighatnasab, M., Kretzschmar, J., Block, K. and Quaas, J. (2022). Impact of holuhraun volcano aerosols on clouds in cloud-system-resolving simulations, *Atmospheric Chemistry and Physics* **22**(13): 8457–8472.

Hegerl, G. C., Crowley, T. J., Baum, S. K., Kim, K.-Y. and Hyde, W. T. (2003). Detection of volcanic, solar and greenhouse gas signals in paleo-reconstructions of northern hemispheric temperature, *Geophysical Research Letters* **30**(5).

Hersbach, H., Bell, B., Berrisford, P., Hirahara, S., Horányi, A., Muñoz-Sabater, J., Nicolas, J., Peubey, C., Radu, R., Schepers, D., Simmons, A., Soci, C., Abdalla, S., Abellan, X., Balsamo, G., Bechtold, P., Biavati, G., Bidlot, J., Bonavita, M., De Chiara, G., Dahlgren, P., Dee, D., Diamantakis, M., Dragani, R., Flemming, J., Forbes, R., Fuentes, M., Geer, A., Haimberger, L., Healy, S., Hogan, R. J., Hólm, E.,

https://doi.org/10.5194/egusphere-2026-578
Preprint. Discussion started: 6 February 2026

Janisková, M., Keeley, S., Laloyaux, P., Lopez, P., Lupu, C., Radnoti, G., de Rosnay, P., Rozum, I., Vamborg, F., Villaume, S. and Thépaut, J.-N. (2020). The ERA5 global reanalysis, *Quarterly Journal of the Royal Meteorological Society* **146**(730): 1999–2049.
URL: *https://rmets.onlinelibrary.wiley.com/doi/abs/10.1002/qj.3803*

Hommel, R., Timmreck, C. and Graf, H. F. (2011). The global middle-atmosphere aerosol model maecham5-sam2: comparison with satellite and in-situ observations, *Geoscientific Model Development* **4**(3): 809–834.
URL: *http://www.geosci-model-dev.net/4/809/2011/*

Hurrell, J. W., Hack, J. J., Shea, D., Caron, J. M. and Rosinski, J. (2008). A new sea surface temperature and sea ice boundary dataset for the community atmosphere model, *Journal of Climate* **21**(19): 5145–5153.
URL: *https://doi.org/10.1175/2008JCLI2292.1*

Karagulian, F., Clarisse, L., Clerbaux, C., Prata, A. J., Hurtmans, D. and Coheur, P.-F. (2010). Detection of volcanic so2, ash, and h2so4 using the infrared atmospheric sounding interferometer (iasi), *Journal of Geophysical Research: Atmospheres* **115**(D2).

Knepp, T. N., Kovilakam, M., Thomason, L. and Miller, S. J. (2024). Characterization of stratospheric particle size distribution uncertainties using sage ii and sage iii/iss extinction spectra, *Atmospheric Measurement Techniques* **17**(7): 2025–2054.

Kokkola, H., Korhonen, H., Lehtinen, K. E. J., Makkonen, R., Asmi, A., Järvenoja, S., Anttila, T., Partanen, A.-I., Kulmala, M., Järvinen, H., Laaksonen, A. and Kerminen, V.-M. (2008). SALSA: a sectional aerosol module for large scale applications, *Atmospheric Chemistry and Physics* **8**(9): 2469–2483.
URL: *http://www.atmos-chem-phys.net/8/2469/2008/*

Kremser, S., Thomason, L. W., von Hobe, M., Hermann, M., Deshler, T., Timmreck, C., Toohey, M., Stenke, A., Schwarz, J. P., Weigel, R., Fueglistaler, S., Prata, F. J., Vernier, J.-P., Schlager, H., Barnes, John E. a nd Antuña-Marrero, J.-C., Fairlie, D., Palm, M., Mahieu, E., Notholt, J., Rex, M., Bingen, C., Vanhellemont, F., Bourassa, A., Plane, J. M. C., Klocke, D., Carn, S. A., Clarisse, L., Trickl, T., Neely, R., James, A. D., Rieger, L., Wilson, J. C. and Meland, B. (2016). Stratospheric aerosol—observations, processes, and impact on climate, *Reviews of Geophysics* **54**(2): 278–335.

Laakso, A., Niemeier, U., Visioni, D., Tilmes, S. and Kokkola, H. (2022). Dependency of the impacts of geoengineering on the stratospheric sulfur injection strategy–part 1: Intercomparison of modal and sectional aerosol modules, *Atmospheric Chemistry and Physics* **22**(1): 93–118.

Laakso, A., Visioni, D., Niemeier, U., Tilmes, S. and Kokkola, H. (2024). Dependency of the impacts of geoengineering on the stratospheric sulfur injection strategy–part 2: How changes in the hydrological cycle depend on the injection rate and model used, *Earth System Dynamics* **15**(2): 405–427.

Lacis, A., Hansen, J. and Sato, M. (1992). Climate forcing by stratospheric aerosols, *Geophysical Research Letters* **19**(15): 1607–1610.

Lurton, T., Jégou, F., Berthet, G., Renard, J.-B., Clarisse, L., Schmidt, A., Brogniez, C. and Roberts, T. J. (2018). Model simulations of the chemical and aerosol microphysical evolution of the sarychev peak 2009 eruption cloud compared to in situ and satellite observations, *Atmospheric Chemistry and Physics* **18**(5): 3223–3247.

Määttänen, A., Merikanto, J., Henschel, H., Duplissy, J., Makkonen, R., Ortega, I. K. and Vehkamäki, H. (2018). New parameterizations for neutral and ion-induced sulfuric acid-water particle formation in nucleation and kinetic regimes, *Journal of Geophysical Research: Atmospheres* **123**(2): 1269–1296.

Malavelle, F. F., Haywood, J. M., Jones, A., Gettelman, A., Clarisse, L., Bauduin, S., Allan, R. P., Karset, I. H. H., Kristjánsson, J. E., Oreopoulos, L. et al. (2017). Strong constraints on aerosol–cloud interactions from volcanic eruptions, *Nature* **546**(7659): 485–491.

https://doi.org/10.5194/egusphere-2026-578
Preprint. Discussion started: 6 February 2026

Malinina, E., Rozanov, A., Niemeier, U., Peglow, S., Arosio, C., Wrana, F., Timmreck, C., von Savigny, C. and Burrows, J. P. (2021). Changes in stratospheric aerosol extinction coefficient after the 2018 ambae eruption as seen by omps-lp and echam5-ham, *Atmospheric Chemistry and Physics* **21**: 14871–14891.

Marshall, L., Johnson, J. S., Mann, G. W., Lee, L., Dhomse, S. S., Regayre, L., Yoshioka, M., Carslaw, K. S. and Schmidt, A. (2019). Exploring how eruption source parameters affect volcanic radiative forcing using statistical emulation, *Journal of Geophysical Research: Atmospheres* **124**(2): 964–985.
URL: *https://agupubs.onlinelibrary.wiley.com/doi/abs/10.1029/2018JD028675*

Marshall, L. R., Maters, E. C., Schmidt, A., Timmreck, C., Robock, A. and Toohey, M. (2022). Volcanic effects on climate: recent advances and future avenues, b. volcanol., 84, 54.

McCormick, M. P., Thomason, L. W. and Trepte, C. R. (1995). Atmospheric effects of the mt pinatubo eruption, *Nature* **373**(6513): 399–404.

McGraw, M. C., Barnes, E. A. and Deser, C. (2016). Reconciling the observed and modeled southern hemisphere circulation response to volcanic eruptions, *Geophysical Research Letters* **43**(13): 7259–7266.

Neely III, R. and Schmidt, A. (2016). Volcaneesm (volcanic emissions for earth system models): Volcanic sulphur dioxide (so2) emissions database from 1850 to present, Centre for Environmental Data Analysis, http://catalogue.ceda.ac.uk/uuid/bfbd5ec825fa422f9a858b14ae7b2a0d. Last accessed 22 March 2023.

Niemeier, U., Riede, F. and Timmreck, C. (2021). Simulation of ash clouds after a laacher see-type eruption, *Climate of the Past* **17**(2): 633–652.
URL: *https://cp.copernicus.org/articles/17/633/2021/*

Niemeier, U. and Schmidt, H. (2017). Changing transport processes in the stratosphere by radiative heating of sulfate aerosols, *Atmospheric Chemistry and Physics* **17**(24): 14871–14886.
URL: *https://www.atmos-chem-phys.net/17/14871/2017/*

Niemeier, U. and Timmreck, C. (2015). What is the limit of climate engineering by stratospheric injection of SO2?, *Atmospheric Chemistry and Physics* **15**(16): 9129–9141.
URL: *http://www.atmos-chem-phys.net/15/9129/2015/*

Niemeier, U., Timmreck, C., Graf, H.-F., Kinne, S., Rast, S. and Self, S. (2009). Initial fate of fine ash and sulfur from large volcanic eruptions, *Atmospheric Chemistry and Physics* **9**(22): 9043–9057.
URL: *http://www.atmos-chem-phys.net/9/9043/2009/*

Niemeier, U., Wallis, S., Timmreck, C., van Pham, T. and von Savigny, C. (2023). How the hunga tonga hunga ha'apai water vapor cloud impacts its transport through the stratosphere: Dynamical and radiative effects, *Geophysical Research Letters* **50**(24): e2023GL106482.

Pohl, C., Wrana, F., Rozanov, A., Deshler, T., Malinina, E., von Savigny, C., Rieger, L. A., Bourassa, A. E. and Burrows, J. P. (2024). Stratospheric aerosol characteristics from sciamachy limb observations: two-parameter retrieval, *Atmospheric Measurement Techniques* **17**(13): 4153–4181.

Quaglia, I., Timmreck, C., Niemeier, U., Visioni, D., Pitari, G., Brodowsky, C., Brühl, C., Dhomse, S. S., Franke, H., Laakso, A. et al. (2023). Interactive stratospheric aerosol models' response to different amounts and altitudes of so 2 injection during the 1991 pinatubo eruption, *Atmospheric Chemistry and Physics* **23**(2): 921–948.

Rieger, L. A., Bourassa, A. E. and Degenstein, D. A. (2014). Stratospheric aerosol particle size information in odin-osiris limb scatter spectra, *Atmospheric Measurement Techniques* **7**(2): 507–522.

Robock, A. (2000). Volcanic eruptions and climate, *Rev. Geophys.* **38**: 191–219.

https://doi.org/10.5194/egusphere-2026-578
Preprint. Discussion started: 6 February 2026

Rozanov, A., Pohl, C., Arosio, C., Bourassa, A., Bramstedt, K., Malinina, E., Rieger, L. and Burrows, J. P. (2024). Retrieval of stratospheric aerosol extinction coefficients from sun-normalized ozone mapper and profiler suite limb profiler (omps-lp) measurements, *Atmospheric Measurement Techniques* **17**(22): 6677–6695.

Rybin, A., Chibisova, M., Webley, P., Steensen, T., Izbekov, P., Neal, C. and Realmuto, V. (2011). Satellite and ground observations of the june 2009 eruption of sarychev peak volcano, matua island, central kuriles, *Bulletin of Volcanology* **73**(9): 1377–1392.

Schmidt, A., Mills, M. J., Ghan, S., Gregory, J. M., Allan, R. P., Andrews, T., Bardeen, C. G., Conley, A., Forster, P. M., Gettelman, A., Portmann, R. W., Solomon, S. and Toon, O. B. (2018). Volcanic radiative forcing from 1979 to 2015, *Journal of Geophysical Research: Atmospheres* **123**(22): 12491–12508.

Sellitto, P., Salerno, G., Corradini, S., Xueref-Remy, I., Riandet, A., Bellon, C., Khaykin, S., Ancellet, G., Lolli, S., Welton, E. J., Boselli, A., Sannino, A., Cuesta, J., Guermazi, H., Eremenko, M., Merucci, L., Stelitano, D. and Guerrieri, L. a. (2023). Volcanic emissions, plume dispersion, and downwind radiative impacts following mount etna series of eruptions of february 21–26, 2021, *Journal of Geophysical Research: Atmospheres* **128**(6): e2021JD035974.

Sofieva, V. F., Rozanov, A., Szelag, M., Burrows, J. P., Retscher, C., Damadeo, R., Degenstein, D., Rieger, L. A. and Bourassa, A. (2024). Crest: a climate data record of stratospheric aerosols, *Earth System Science Data* **16**(11): 5227–5241.

Solomon, S. (1999). Stratospheric ozone depletion: A review of concepts and history, *Reviews of Geophysics* **37**(3): 275–316.

Solomon, S., Daniel, J. S., Neely III, R. R., Vernier, J.-P., Dutton, E. G. and Thomason, L. W. (2011). The persistently variable "background" stratospheric aerosol layer and global climate change, *Science* **333**(6044): 866–870.

Stier, P., Feichter, J., Kinne, S., Kloster, S., Vignati, E., Wilson, J., Ganzeveld, L., Tegen, I., Werner, M., Balkanski, Y., Schulz, M., Boucher, O., Minikin, A. and Petzold, A. (2005). The aerosol–climate model ECHAM5–HAM, *Atmos. Chem. Phys.* **5**: 1125–1156.

Sukhodolov, T., Sheng, J.-X., Feinberg, A., Luo, B.-P., Peter, T., Revell, L., Stenke, A., Weisenstein, D. K. and Rozanov, E. (2018). Stratospheric aerosol evolution after pinatubo simulated with a coupled size-resolved aerosol–chemistry–climate model, socol-aerv1.0, *Geoscientific Model Development* **11**(7): 2633–2647.
URL: *https://gmd.copernicus.org/articles/11/2633/2018/*

Tilmes, S., Mills, M. J., Zhu, Y., Bardeen, C. G., Vitt, F., Yu, P., Fillmore, D., Liu, X., Toon, B. and Deshler, T. (2023). Description and performance of a sectional aerosol microphysical model in the community earth system model (cesm2), *Geoscientific Model Development* **16**(21): 6087–6125.
URL: *https://gmd.copernicus.org/articles/16/6087/2023/*

Timmreck, C. (2012). Modeling the climatic effects of large explosive volcanic eruptions, *WIREs Climate Change* **3**(6): 545–564.

Timmreck, C. and Graf, H.-F. (2006). The initial dispersal and radiative forcing of a northern hemisphere mid–latitude super volcano: A model study, *Atmos. Chem. Phys.* **6**: 35–49.
URL: *http://www.atmos-chem-phys.net/6/35/2006/*

Toohey, M., Krüger, K., Bittner, M., Timmreck, C. and Schmidt, H. (2014). The impact of volcanic aerosol on the northern hemisphere stratospheric polar vortex: mechanisms and sensitivity to forcing structure, *Atmospheric Chemistry and Physics* **14**(23): 13063–13079.
URL: *https://www.atmos-chem-phys.net/14/13063/2014/*

Waythomas, C. F., Scott, W. E., Prejean, S. G., Schneider, D. J., Izbekov, P. and Nye, C. J. (2010). The 7–8 august 2008 eruption of kasatochi volcano, central aleutian islands, alaska, *Journal of Geophysical Research: Solid Earth* **115**(B12).

https://doi.org/10.5194/egusphere-2026-578
Preprint. Discussion started: 6 February 2026

Wrana, F., Niemeier, U., Thomason, L. W., Wallis, S. and von Savigny, C. (2023). Stratospheric aerosol size reduction after volcanic eruptions, *Atmospheric Chemistry and Physics* **23**(17): 9725–9743.
URL: *https://acp.copernicus.org/articles/23/9725/2023/*

Wrana, F., Von Savigny, C., Zalach, J. and Thomason, L. W. (2021). Retrieval of stratospheric aerosol size distribution parameters using satellite solar occultation measurements at three wavelengths, *Atmospheric Measurement Techniques* **14**(3): 2345–2357.

Zanchettin, D., Khodri, M., Timmreck, C., Toohey, M., Schmidt, A., Gerber, E., Hegerl, G., Robock, A., Pausata, F., Ball, W., Bauer, S., Bekki, S., Dhomse, S., LeGrande, A., Mann, G., Marshall, L., Mills, M., Marchand, M., Niemeier, U., Poulain, V., Rozanov, E., Rubino, A., Stenke, A., Tsigaridis, K. and Tummon, F. (2016). The model intercomparison project on the climatic response to volcanic forcing (volmip): experimental design and forcing input data for cmip6, *Geoscientific Model Development* **9**(8): 2701–2719.
URL: *https://www.geosci-model-dev.net/9/2701/2016/*

Zhu, Y., Toon, O. B., Jensen, E. J., Bardeen, C. G., Mills, M. J., Tolbert, M. A., Yu, P. and Woods, S. (2020). Persisting volcanic ash particles impact stratospheric so2 lifetime and aerosol optical properties, *Nature communications* **11**(1): 4526.

Zhu, Y., Toon, O. B., Kinnison, D., Harvey, V. L., Mills, M. J., Bardeen, C. G., Pitts, M., Bègue, N., Renard, J.-B., Berthet, G. and Jegou, F. (2018). Stratospheric aerosols, polar stratospheric clouds, and polar ozone depletion after the mount calbuco eruption in 2015, *Journal of Geophysical Research: Atmospheres* **123**(21): 12–308.